Korean J. Chem. Eng., **31**(12), 2162-2169 (2014)
DOI: 10.1007/s11814-014-0167-3

pISSN: 0256-1115
eISSN: 1975-7220

Production of elemental sulfur and ammonium thiosulfate by H_2S oxidation over Nb_2O_5 supported on Fe-pillared clay

Moon-Il Kim, Goo-Hwa Lee, Dong-Woo Kim, Dong-Heon Kang, and Dae-Won Park†

School of Chemical and Biomolecular Engineering, Pusan National University, Busan 609-735, Korea
(*Received 5 April 2014 • accepted 16 June 2014*)

Abstract−The catalytic oxidation of hydrogen sulfide (H_2S) in the presence of ammonia was studied over niobium pentoxide supported on Fe-pillared clay catalysts (Nb/Fe-PILCs). The synthesized catalysts were characterized by various techniques such as X-ray diffraction, BET method, X-ray photoelectron spectroscopy, temperature-programmed reduction, temperature-programmed desorption of ammonia, and transmission electron microscopy. Catalytic performance studies of the Nb/Fe-PILC catalysts showed that H_2S was successfully converted to elemental sulfur and ammonium thiosulfate without any considerable emission of sulfur dioxide. The results show that 3 wt% Nb/Fe-PILC exhibited the highest H_2S conversion, which might be due to the uniform dispersion of niobium-oxide species on the Fe-PILC support. Niobium on the fresh Nb/Fe-PILC catalyst was in the +5 oxidation state and it was partially reduced to a lower oxidation state after the reaction.

Keywords: Selective Oxidation, Hydrogen Sulfide, Sulfur, Pillared Clay, Niobium Oxide

INTRODUCTION

Hydrogen sulfide (H_2S) is a common by-product of fuels in oil and gas refinery processes. It is highly odorous and toxic. Recovery of S is a major issue in emission reduction because of the stringent fuel regulations, increasing environmental concerns, and the need to process sour crude oils and natural gases. For many years, H_2S has been removed from petroleum refineries and natural gas plants by the well-known Claus process [1]. However, 3-5% of H_2S cannot be converted to S because of thermodynamic limitations.

Various commercial processes based on adsorption, absorption, and wet oxidation have been used to treat tail gases containing low concentrations (<5 vol%) of S from Claus plants or other emission sources. Among these processes, dry catalytic oxidation of H_2S to elemental sulfur after the hydrogenation of the S-containing gas to H_2S has attracted considerable attention. Two commercially developed processes that are based on the direct oxidation of H_2S to elemental sulfur are the Mobil direct oxidation process (MODOP) [2,3] and Super Claus process [1,4]. In the MODOP process, H_2S is oxidized to elemental sulfur with a stoichiometric amount of oxygen over a TiO_2 catalyst. However, one disadvantage of the MODOP process is that the presence of water deactivates the catalyst, and hence, the tail gas should be treated with a dehydration step prior to the reaction. In the Super Claus process, the tail gas can be treated without a dehydration step because the Fe-based catalyst is resistant to water; however, this process requires excess oxygen (ten-times the stoichiometric amount).

Although the oxidation of H_2S to elemental sulfur has been widely studied [5], there are no reports on its vapor-phase conversion in the presence of H_2O and NH_3. A mixture of H_2S, NH_3, and water vapor is released during the steel-smelting process, where H_2S from a coke oven is generally scrubbed and concentrated using an aqueous NH_3 solution. The concentrated H_2S is separated from the solution and transferred to the Claus plant. However, because of the incomplete separation of H_2S from the solution, the remaining aqueous NH_3 stream contains approximately 2% H_2S, which causes SO_x emission problems during incineration. Hence, new technologies are being developed to remove H_2S from these types of streams.

One approach for resolving this problem is the selective catalytic oxidation of H_2S to ammonium thiosulfate (ATS) and elemental sulfur. We previously reported a vapor-phase catalytic process for the selective conversion of H_2S in a stream containing NH_3 and H_2O [6-10]. ATS is used in photography and agricultural applications. The conventional processes for the production of ATS are based on liquid-phase reactions. The ATS Claus tail gas clean-up process is divided into two sections: 1) absorption of SO_2 from the incinerator in aqueous NH_3, and 2) conversion of the intermediate product to ATS by sparging H_2S into the converter. In another process, H_2SO_4 is reacted with aqueous NH_3 solution below 45 °C and the mixture is reacted with H_2S to form ATS. Note that the proposed technique has the advantage of direct vapor-phase operation when compared to the above-mentioned approaches.

Considerable attention is being paid to the development of novel materials for various catalytic applications. Among them, clays and clay minerals have attracted attention owing to their abundance, low cost, and unique properties. However, the low porosity and poor thermal stability of clays have restricted their use as catalysts. The aforementioned properties can be improved through certain modifications; one such modification is pillaring, which results in high porosity and high thermal stability. Pillared interlayered clays (PILCs) are two-dimensional zeolite-like materials, which are synthesized by replacing the charge-compensating cations between the clay layers with large polymeric or oligomeric hydroxy metal cations formed by the hydrolysis of metal oxides or metal salts. The metal hydroxy

†To whom correspondence should be addressed.
E-mail: dwpark@pusan.ac.kr

cations undergo dehydration and dehydroxylation upon heating, resulting in the formation of stable metal-oxide clusters. These clusters act as pillars that maintain the separation of silicate layers and they generate an interlayer space of molecular dimensions [11-17]. Compared to zeolites, PILCs are advantageous because new materials can be tailored to particular applications by varying the size, separation, and composition of the pillars.

Niobium compounds are important catalysts for various reactions [18]. Because the electronegativity and ionic radius of Nb are different from those of its neighbors (V, Zr, Mo) in the periodic table, the catalytic behavior of Nb compounds is quite different from those of the surrounding elements' compounds [18].

Several studies have also reported the selective catalytic oxidation of H_2S using a variety of catalysts [19-27]. In our previous study [6,13,28-30], we reported the catalytic performance of vanadia-supported pillared clay for the selective catalytic oxidation of H_2S to elemental sulfur. We here report the preparation of Nb_2O_5-supported on Fe-pillared clay. The synthesized materials have been characterized and their catalytic performance in the selective oxidation of H_2S has been investigated. In addition, their performance in the production of elemental sulfur and ATS in the presence of NH_3 was also studied.

EXPERIMENTAL

1. Catalyst Synthesis

The starting material was Na-montmorillonite (Na-MMT, Kunipia-F, Kunimine Industrial Company) with a cation exchange capacity of 120 meq/100 g. $FeCl_3 \cdot 6H_2O$ (97%, Aldrich) was used for the synthesis of polymeric hydroxyl-iron(III) cations. The pillaring solution was obtained by the slow addition of 0.4-M NaOH solution to a 0.2-M $FeCl_3$ solution to obtain the required OH/Fe molar ratio of 2. The mixture was stirred for 6 h at room temperature. The pillaring process was performed with clay slurry (2 wt%). The pillaring solution was added dropwise to the clay suspension at 40 °C with stirring. An Fe/clay ratio of 60 mmol/g was obtained. The slurry was stirred for 24 h at room temperature. After aging for 12 h, the product was filtered and washed with distilled water. It was then dried in air and calcined at 400 °C for 3 h under air flow. The obtained Fe-PILC product was used as the support.

Niobium oxide-loaded Fe-PILC samples containing 1, 2, 3, 5, and 8 wt% niobium oxide were prepared by the wet impregnation process. Ammonium niobate(V) oxalate hydrate (99.99%, Aldrich) was used as the precursor compound. Fe-PILC was impregnated with the aqueous precursor solution. All the samples were dried at 80 °C for 20 h and were calcined at 400 °C for 3 h. The samples were labeled as *x* wt% Nb/Fe-PILC, where *x* refers to the niobium oxide loaded onto the support.

2. Characterization of Catalysts

The chemical composition of the samples was determined by X-ray fluorescence (XRF, Philips PW 2400) and inductively coupled plasma optical emission spectroscopy (ICP-OES, JOBIN YVON).

The X-ray diffraction (XRD) patterns were obtained on a Bruker Advanced D8 powder diffractometer using Ni-filtered Cu Kα radiation (λ=1.5404 Å). A fixed power source (40 kV, 300 mA) and a scan speed of 0.02° 2θ min^{-1} were applied to determine the XRD patterns.

The surface areas were determined by N_2 adsorption at 77 K using a Micromeritics ASAP 2010 instrument. Prior to N_2 adsorption, the samples were outgassed under vacuum for 12 h at 110 °C. The specific surface areas were calculated using the BET equation, and the total pore volumes were evaluated from the N_2 uptake at a relative pressure of P/P_0=0.99.

X-ray photoelectron spectroscopy (XPS) analyses were performed using an X-ray photoelectron spectrometer (VG, ESCALAB 250) with monochromatic Al Kα radiation (hυ=1,486.6 eV). The samples were calcined at 400 °C for 3 h and pressed into self-supporting wafers without a binder; they were then pretreated under an ultra-high vacuum. The binding energies (BE) were calculated using C 1s as the reference (284.6 eV) band.

Temperature-programmed reduction by H_2 (H_2-TPR) was performed with a BEL-CAT chemisorption apparatus (BEL, JAPAN). For H_2-TPR, approximately 50 mg of the sample was pretreated in an oxidative atmosphere (5% O_2 in He) at 400 °C for 30 min. After cooling to room temperature, the H_2-TPR (5% in He, flow rate 20 mL/min) was performed from 100 to 700 °C at a heating rate of 10 °C/min.

Temperature-programmed desorption of ammonia (NH_3-TPD) was performed with a BEL-CAT chemisorption apparatus (BEL, JAPAN). For NH_3-TPD, approximately 50 mg of the sample was pretreated at 400 °C for 2 h under He flow and was cooled to ambient temperature. Pure NH_3 gas (50 mL/min) was adsorbed at 100 °C for 20 min. Desorption was carried out with a linear heating rate of 10 °C/min at a He flow rate of 20 mL/min.

Transmission electron microscopy (TEM) analysis was performed using a JEOL 2011 electron microscope fitted with a lanthanum hexaboride (LaB_6) filament and operated at 200 kV.

3. Reaction Tests

The reaction tests were performed in a continuous flow fixed-bed reactor made from a Pyrex tube with 1-inch internal diameter. A gaseous mixture of H_2S, O_2, NH_3, and a balance of He (purity of 50%, 98%, 99.9%, and 99.999%, respectively) was used. To condense the solid products (S and ATS), a condenser was attached to the effluent side of the reactor and its temperature was maintained at 110 °C. A line filter was installed after the condenser to trap any solid mist that was not captured by the condenser. All the lines and fittings from the condenser to the gas chromatograph (GC) were heated above 120 °C to prevent condensation of the water vapor. The gas flow rate was controlled with mass flow controllers (Brooks MFC, 5850E). In a typical experiment, the reactant composition consisted of 5 vol% H_2S, 2.5 vol% O_2, 5 vol% NH_3, and the remaining composition consisted of He. The gas hourly space velocity (GHSV) was fixed at 10,000 h^{-1}.

The content of the effluent gas was analyzed by a GC (HP 5890) containing a 1.8-m Porapak T column (80-100 mesh) equipped with a thermal conductivity detector at 100 °C. The exit gas from the analyzer was passed through a trap containing concentrated NaOH solution and was vented to a hood. The % conversion of H_2S and the % selectivity toward SO_2, S, and ATS are defined as follows:

$$\text{Conversion of } H_2S = \frac{[H_2S]_{inlet} - [H_2S]_{outlet}}{[H_2S]_{inlet}} \times 100(\%)$$

$$\text{Selectivity to a special product } (SO_2, S, ATS) = \frac{[\text{Product}]_{outlet}}{[H_2S]_{inlet} - [H_2S]_{outlet}} \times 100(\%)$$

Table 1. Chemical composition (wt%) of the initial clay, Fe-PILC, and Nb/Fe-PILCs

Sample	Si	Al	Fe	Na	Mg	Nb
Na-MMT	56.7	29.2	2.2	4.5	5.8	-
PILC	36	9.7	53	0.1	0.8	-
1 wt% Nb/Fe-PILC	34	11	53	0.1	1.5	1.2
2 wt% Nb/Fe-PILC	30	9.7	57	0.2	0.5	2.3
3 wt% Nb/Fe-PILC	29	1	58	0.1	0.1	3
5 wt% Nb/Fe-PILC	31	9.1	53	0.3	0.7	5.2
8 wt% Nb/Fe-PILC	27	9.5	54	0.2	0.6	8.1

Because one mole of ATS is obtained from two moles of H_2S, the ATS selectivity was calculated by multiplying the number of moles of ATS by two.

RESULTS AND DISCUSSIONS

1. Characterization of Catalysts

1-1. Chemical Composition

Table 1 shows the chemical compositions of the initial clay, Fe-PILC, and Nb/Fe-PILCs. The pillaring of the initial clay by Fe_2O_3 increased the Fe_2O_3 content with a replacement of the interlayer Na cations. The relative amounts of Si, Al, and Mg remained nearly constant in all the samples after pillaring. This suggests that the composition of the clay sheet is preserved in Fe-PILC and Nb/Fe-PILCs.

1-2. X-ray Diffraction

Fig. 1 shows the low-angle XRD patterns of Na-MMT and Fe-PILC calcined at 400 °C. The Na-MMT shows a major peak at a 2θ of 7°, which is usually assigned to the basal (001) reflection (d(001)). In the Fe-PILC, the d(001) peak was found to shift toward a lower 2θ, which indicates the expansion of the layered structure because of pillaring [31-33]. A diffraction peak of (001) reflection of Na-MMT was absent in the pillared clay sample. This shows that iron-oxide pillars are well distributed in the clay and that the product has no contribution from the unpillared regions. Large and hydrated Fe polyoxocations introduced into the interlayer spaces of the clay pushed the sheets apart and increased the d-spacing. Calcination of Fe-intercalated clays led to the dehydration and dehydroxylation of Fe polycations and formation of polymeric Fe_2O_3 species that permanently links the adjacent layers [33]. The d-spacing of the Fe-PILC calcined at 400 °C was found to be 63 Å.

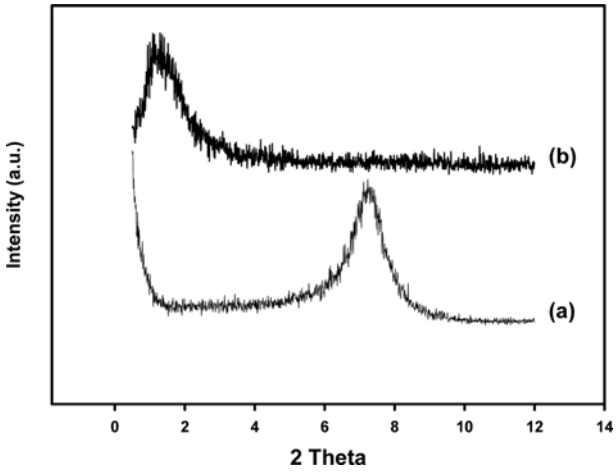

Fig. 1. Low-angle XRD patterns: (a) Na-MMT, (b) Fe-PILC.

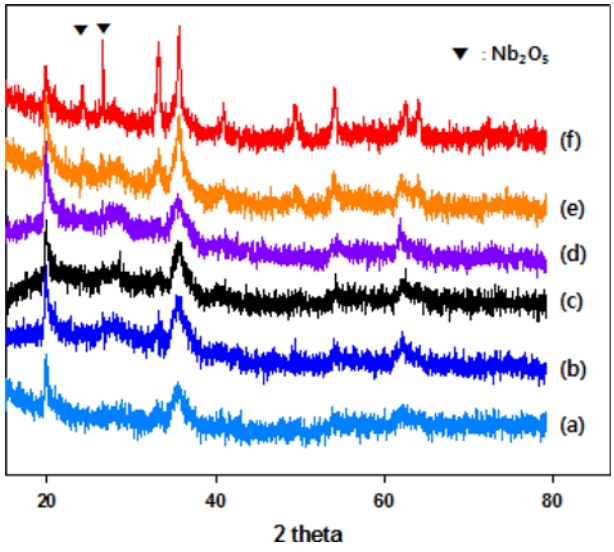

Fig. 2. High-angle XRD patterns: (a) Fe-PILC, (b) 1 wt% Nb/Fe-PILC, (c) 2 wt% Nb/Fe-PILC, (d) 3 wt% Nb/Fe-PILC (e) 5 wt% Nb/Fe-PILC, (f) 8 wt% Nb/Fe-PILC.

Fig. 2 shows the high-angle XRD patterns of the Fe-PILC and Nb/Fe-PILC catalysts. The XRD patterns of Fe-PILC after impregnation with niobium oxides were similar to that of Fe-PILC. This suggests that niobium oxides are well dispersed on the support. However, small peaks that represent the crystalline niobium oxides were observed at Nb contents higher than 5 wt% Nb/Fe-PILC.

1-3. Textural Properties of Fe-PILC and Nb/Fe-PILCs

The textural properties of pillared clays mainly depend upon the nature of the pillars between the clay sheets, preparation method, and calcination temperature. Table 2 shows the textural data obtained from the BET surface area analysis. The BET surface area of Fe-PILC was 206 m^2/g, whereas that of the initial clay was only 26 m^2/g. The large increase in the surface area of Fe-PILC indicates the successful pillaring of Fe_2O_3 species into the silicate layers of the clay [32]. During the pillaring process, the expansion of the clay structure and the desegregation of the clay particles largely con-

Table 2. Specific surface area (S_{BET}), total pore volume (V_P), mesopore volume (V_{MP}), micropore volume ($V_{\mu P}$) and average pore size (D_P) of the initial clay, Fe-PILC, and Nb/Fe-PILCs

Sample	S_{BET} (m^2/g)	V_P (cm^3/g)	V_{MP} (cm^3/g)	$V_{\mu P}$ (cm^3/g)	D_P (nm)
Na-MMT	26	-	-	-	-
PILC	206	0.256	0.252	0.004	-
1 wt% Nb/Fe-PILC	178	0.222	0.216	0.006	37.2
2 wt% Nb/Fe-PILC	166	0.217	0.215	0.002	36.8
3 wt% Nb/Fe-PILC	141	0.214	0.213	0.001	37.3
5 wt% Nb/Fe-PILC	122	0.191	0.190	0.001	36.7
8 wt% Nb/Fe-PILC	115	0.187	0.186	0.001	36.8

Table 3. XPS analysis data: the binding energies of Fe $2p_{3/2}$ and Nb $3d_{5/2}$

Catalyst	Binding energy (eV)	
	Fe $2p_{3/2}$	Nb $3d_{5/2}$
Fe-PILC	711.0	-
1 wt% Nb/Fe-PILC	711.3	207.0
2 wt% Nb/Fe-PILC	711.2	207.1
3 wt% Nb/Fe-PILC	711.9	206.9
5 wt% Nb/Fe-PILC	711.0	207.1
8 wt% Nb/Fe-PILC	711.6	206.9

tributed to the enhancement of both the surface area and porosity of the clays [28,29,34-36]. The high surface area obtained by pillaring allows the dispersion of niobium oxides on the Fe-PILC. However, an increase in the niobium-oxide loading onto the Fe-PILC support decreased the surface area and total pore volume, probably because of pore blockage resulting from progressive filling with niobium-oxide species.

1-4. X-ray Photoelectron Spectroscopy Analysis

XPS is frequently used in catalysis because it provides information about the catalyst surface. In this study, the ratio of niobium oxide to support oxide provides information on the dispersion of the niobium-oxide phase on the support. The surface oxidation states

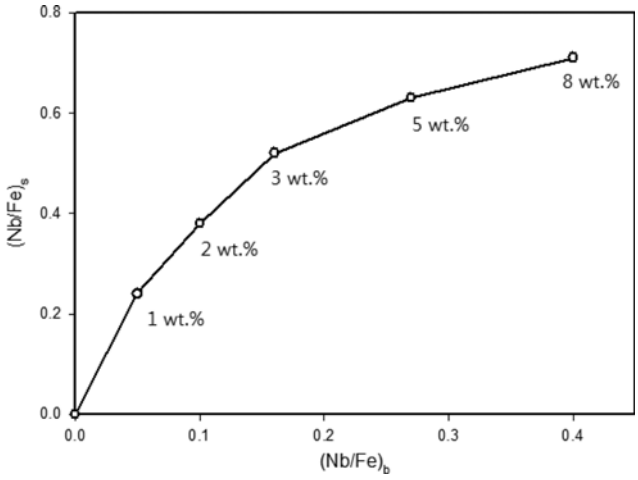

Fig. 3. XPS (Nb/Fe) surface atomic ratio vs. the corresponding (Nb/Fe) bulk ratio.

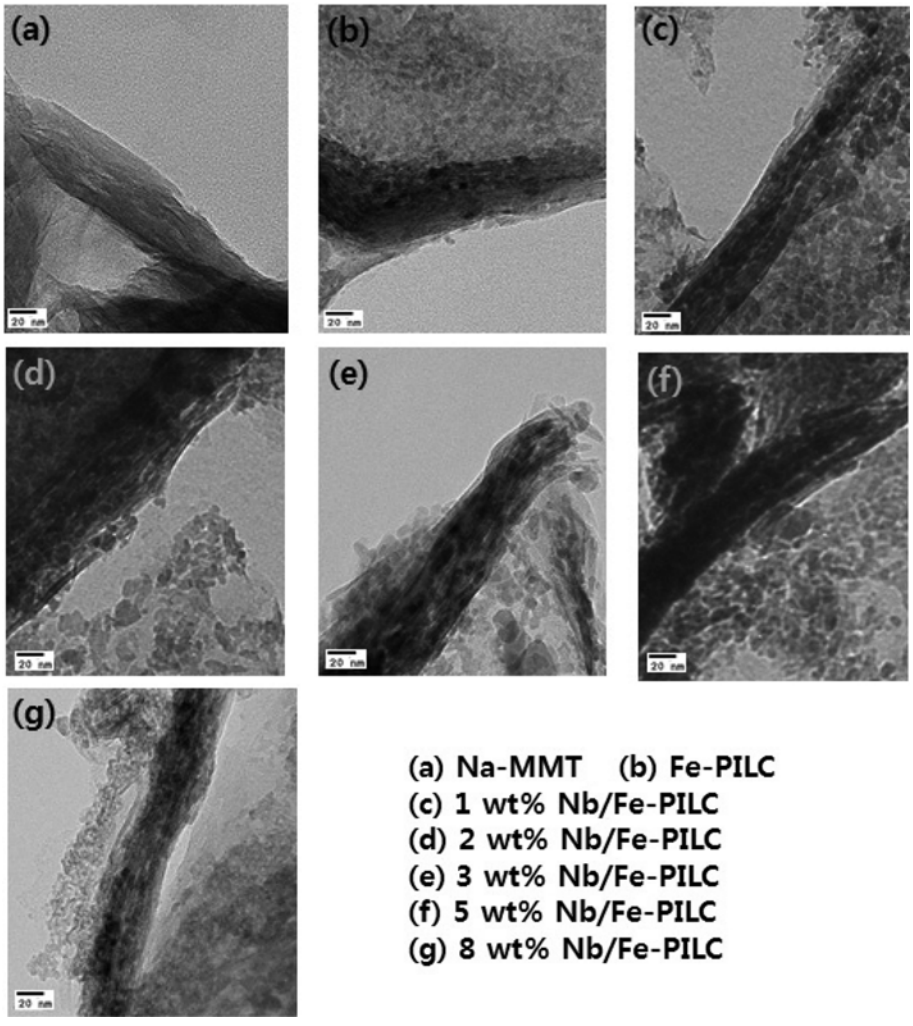

Fig. 4. TEM images of Na-MMT, Fe-PILC, and Nb/Fe-PILCs.

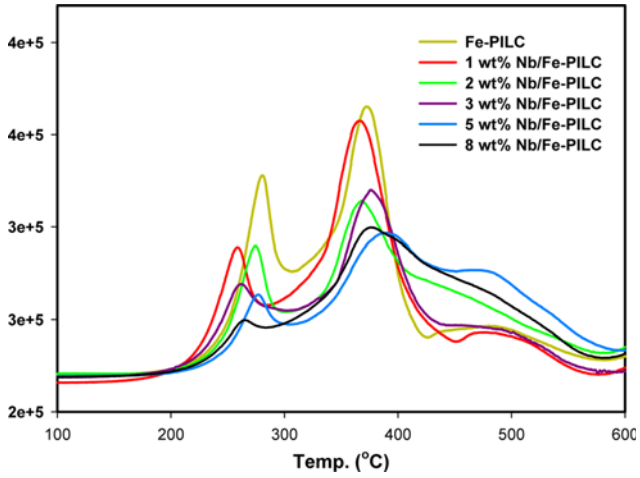

Fig. 5. H_2-TPR profiles of the Fe-PILC and Nb/Fe-PILCs.

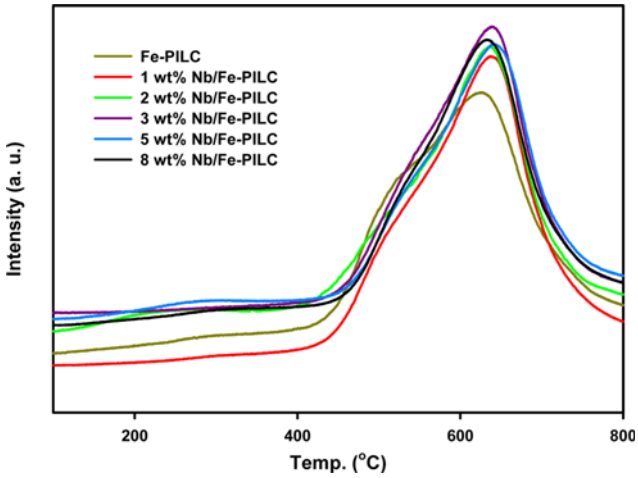

Fig. 6. NH_3-TPD profiles of the Fe-PILC and Nb/Fe-PILCs.

and BE of Nb and Fe were also analyzed by XPS. Table 3 shows the BE of Fe $2p_{3/2}$ and Nb $3d_{5/2}$. The BE of Fe $2p_{3/2}$ for Fe-PILC was observed at 711 eV, which corresponds to Fe in the +3 oxidation state in Fe-PILC. A Nb $3d_{5/2}$ BE of approximately 207 eV was observed for all the Nb/Fe-PILC catalysts. This indicates that most of the Nb occurs as +5 oxidation state on the Fe-PILC support [37-39].

Fig. 3 shows a plot of the XPS surface atomic ratios $(Nb/Fe)_s$ vs. the corresponding bulk ratios $(Nb/Fe)_b$. As the loading increased from 1 to 3 wt%, a linear increase in the surface atomic ratio was observed, which shows a uniform dispersion of Nb on the Fe-PILC up to 3 wt%. For 5 and 8 wt% of niobium-oxide loading, the surface atomic ratio increased slowly, probably because of the formation of polymeric niobium pentoxide (Nb_2O_5) species on the surface.

1-5. Transmission Electron Microscopy Analysis

TEM permits the direct observation of microstructures resulting from the transformation of clay to pillared clay. The TEM images of Na-MMT, Fe-PILC, and Nb/Fe-PILC (1-8 wt%) catalysts are shown in Fig. 4. Comparison of the TEM micrograph of the initial clay with that of Fe-PILC reveals that the clay sheets are well pillared and maintain a layered structure. After niobium-oxide loading, the layered structure was preserved without any noticeable change in the spacing between the clay layers.

1-6. Temperature-programmed Reduction by Hydrogen

The reducibility of the Nb/Fe-PILC catalysts can be evaluated by the H_2-TPR experiment. Fig. 5 shows the TPR profiles of the Nb/Fe-PILC catalysts calcined at 400 °C. It is well known that low reduction temperatures correspond to a high degree of niobium-oxide dispersion. TPR profiles showed three reduction peaks at 230-280 °C (region I), 340-400 °C (region II), and 450-550 °C (region III). When the Nb loading was below 3 wt%, the reduction peaks of regions I and II were higher than those of Nb/Fe-PILCs with higher loading (5 and 8 wt%), indicating the facile reduction of finely dispersed niobium oxide on the surface. However, the peaks at region III were much bigger for high-loading catalysts compared to those of the low-loading catalysts. This phenomenon arises because of the formation of Nb_2O_5 crystals, as observed in the XRD analysis. At low Nb content, most of the Nb atoms interact with the Fe-PILC support, leading to higher reducibility. As the niobium-oxide loading increases, a higher proportion of the surface Nb atoms interacts with the internal Nb layer. This leads to an increase in the bond strength of the niobyl group, which approaches that of pure Nb_2O_5. This also leads to a higher heterogeneity of the Nb-reduction centers, widening the reduction peak. Therefore, it may be concluded that Nb_2O_5 crystals must be present in the catalyst with higher niobium-oxide content, which is in agreement with the XRD results.

1-7. Temperature-programmed Desorption of Ammonia

Fig. 6 shows the NH_3-TPD profiles of the Fe-PILC and Nb/Fe-PILCs. The pillared clays generally contain both the Brönsted and Lewis acid sites [36,40]. These acid sites arise from the exposure of the clay structure and the introduced pillar metal oxide [35,40,41]. The acid sites in the Fe-PILC could be classified into weak (desorption below 300 °C) and strong (desorption at 600 °C) acid sites. The peak at low temperature is due to the NH_3 desorption from the weak Brönsted acid sites, whereas that at high temperature corresponds to the desorbed NH_3 from the strong Lewis acid sites. The Lewis and Brönsted acid sites present on the Fe-PILC arise from the iron-oxide pillars and structural hydroxyl groups of the MMT layer, respectively. Thus, the Fe-PILC data demonstrated the presence of both Lewis and Brönsted acidities, with the Lewis acid being the dominant species.

The desorption pattern shows that the addition of niobium oxide to the Fe-PILC increases the intensity and maximum peak temperature at the high-temperature region, which indicates an increase in the Lewis acidity. Table 4 summarizes the maximum peak temper-

Table 4. Maximum peak temperature and the amount of NH_3-TPD

	Fe-PILC	1 wt% Nb/Fe-PILC	2 wt% Nb/Fe-PILC	3 wt% Nb/Fe-PILC	5 wt% Nb/Fe-PILC	8 wt% Nb/Fe-PILC
T_{max}	625	634	637	638	637	632
Acid amount (mmol/g)	26.6	31.9	35.9	39.2	32.6	31.6

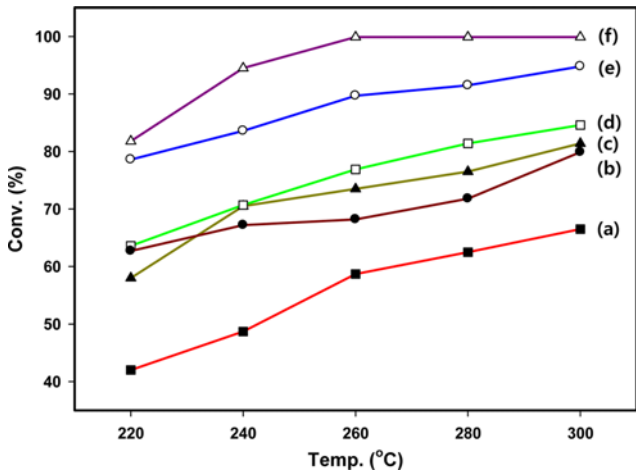

Fig. 7. Conversion of H_2S for Nb/Fe-PILC catalysts at different temperatures: (a) Fe-PILC, (b) 8 wt% Nb/Fe-PILC, (c) 1 wt% Nb/Fe-PILC, (d) 5 wt% Nb/Fe-PILC, (e) 2 wt% Nb/Fe-PILC, (f) 3 wt% Nb/Fe-PILC.

ature and amount of NH_3 desorbed in the TPD. The various quantities of niobium-oxide loading did not influence the peak temperature and NH_3 desorption amount. However, higher values of peak temperature and NH_3 desorption were observed at 3 wt% Nb/Fe-PILC compared to other catalysts.

2. Catalytic Performance

Fig. 7 shows the conversion of H_2S using Nb/Fe-PILC catalysts at the reaction temperature range 220-300 °C, with the reactant composition of $H_2S/O_2/He=5/2.5/92.5$ at GHSV=10,000 h^{-1}. All the Nb/Fe-PILC catalysts showed good catalytic performance for H_2S oxidation. They maintained stable catalytic activities and a slight SO_2 emission was observed. Higher H_2S conversion was discovered at a higher reaction temperature. This trend is similar to that previously observed with supported vanadia catalysts [13,28-31,36-38, 42,43]. The catalytic activity of the niobium oxide-supported catalysts depends on the nature of the surface niobium-oxide species present in the catalyst. An increase in H_2S conversion was observed when the niobium-oxide loading increased from 1 to 3 wt%, probably because of good dispersion of niobium-oxide species on the Fe-PILC support. This result is in good agreement with the XPS data that showed a uniform dispersion of niobium oxide on the surface of Fe-PILC up to a niobium-oxide content of 3 wt%.

A decrease in H_2S conversion was observed at niobium-oxide loading of 5 and 8 wt%, probably because of the formation of a relatively less reactive aggregated form of niobium oxide, which decreased the uniform dispersion on the support. The decrease in the catalytic performance at higher loadings could also be due to the decrease in the specific surface area and pore volume owing to the pore blockage by the niobium oxides.

Table 5 shows the selectivity of Nb/Fe-PILC catalysts to elemental sulfur at temperatures ranging from 220 to 300 °C. It can be observed that the selectivity remained almost constant at 98-99% for all the Nb/Fe-PILC catalysts, despite variation of conversion over a wide range. This suggests that the selectivity of these catalysts to elemental sulfur is less sensitive to temperature.

In the absence of NH_3, the following elementary reactions occurred

Table 5. Selectivity to SO_2 and S at temperatures ranging from 220-300 °C

Catalyst	Temp (°C)	S-SO_2 (%)	S-S (%)
1 wt% Nb/Fe-PILC	220	0.7	99.3
	240	0.5	99.5
	260	0.4	99.6
	280	0.6	99.4
	300	0.5	99.5
2 wt% Nb/Fe-PILC	220	0.4	99.6
	240	0.4	99.6
	260	0.3	99.7
	280	0.2	99.8
	300	0.3	99.7
3 wt% Nb/Fe-PILC	220	0.7	99.3
	240	0.4	99.6
	260	0.9	99.1
	280	0.4	99.6
	300	0.3	99.7
5 wt% Nb/Fe-PILC	220	1.1	98.9
	240	1.0	99.0
	260	1.5	98.5
	280	1.2	98.7
	300	1.1	98.9
8 wt% Nb/Fe-PILC	220	0.6	99.4
	240	0.7	99.3
	260	1.7	98.3
	280	1.3	98.7
	300	1.4	98.6

Reaction comditions: $H_2S/O_2/He=5/2.5/92.5$, GHSV=10,000 h^{-1}, cat.=0.5 g, reaction time=2 h)

in the Claus process:

$$H_2S+1/2\ O_2 \rightarrow 1/n\ S_n+H_2O \quad (1)$$

$$1/n\ S_n+O_2 \rightarrow SO_2 \quad (2)$$

$$H_2S+3/2\ O_2 \rightarrow SO_2+H_2O \quad (3)$$

$$2\ H_2S+SO_2 \rightarrow 3/n\ S_n+2\ H_2O \quad (4)$$

H_2S is converted to elemental sulfur by reaction (1) and partly to SO_2 by reaction (3). SO_2, which is produced by reactions (2) and (3), can be converted to elemental sulfur by the Claus reaction, which has a high selectivity for elemental sulfur. This indicates that the Nb/Fe-PILC is suitable for catalyzing the industrial oxidation of H_2S to elemental sulfur without considerable SO_2 emission.

Table 6 summarizes the H_2S conversion (X-H_2S) and product selectivity (S-SO_2, S-S and S-ATS) for Nb/Fe-PILC catalysts with a reactant composition of $H_2S/O_2/NH_3/He=5/2.5/5/92.5$ at GHSV= 10,000 h^{-1} after 6 h of reaction at 300 °C. Compared to the reactant mixture without NH_3 (Fig. 7), the conversion of H_2S increased by the reaction between H_2S and NH_3. Selectivity of SO_2 decreased because of consumption by NH_3.

Ammonia is known to react with H_2S to form ammonium sulfide [$(NH_4)_2S$], which can be oxidized to produce elemental sulfur.

$$H_2S+2\ NH_3 \leftrightarrow (NH_4)_2S \quad (5)$$

Table 6. H_2S conversion (X-H_2S) and selectivity to products (S-SO_2, S-S and S-ATS) at 300 °C with NH_3

Catalyst	X-H_2S (%)	S-SO_2 (%)	S-S (%)	S-ATS (%)
1 wt% Nb/Fe-PILC	99.1	0.4	91	8.6
2 wt% Nb/Fe-PILC	99.2	0.2	93	6.8
3 wt% Nb/Fe-PILC	99.3	0.1	92	7.9
5 wt% Nb/Fe-PILC	99.7	0.3	95	4.7
8 wt% Nb/Fe-PILC	99.1	0.6	93	6.4

Reaction conditions: $H_2S/O_2/NH_3/He$=5/2.5/5/87.5, GHSV=10,000 h^{-1}, cat.=0.5 g, T=300 °C, reaction time=2 h

$$(NH_4)_2S+1/2\ O_2 \rightarrow S+2\ NH_3+H_2O \quad (6)$$

Hartley and Matterson [42] reported the formation of ammonium bisulfite and ammonium sulfite from the reaction of SO_2 and NH_3 in the presence of H_2O.

$$SO_2+2\ NH_3+H_2O \rightarrow (NH_4)_2SO_3 \quad (7)$$

Zey et al. [43] reported the following reaction for the production of ATS in the Claus tail gas process.

$$H_2S+NH_4HSO_3+(NH_4)_2SO_3 \rightarrow 3/2\ (NH_4)_2S_2O_3+3/2\ H_2O \quad (8)$$

Therefore, SO_2 may be consumed during the formation of ATS. ATS is commercially produced by the reaction of ammonium sulfite with excess S.

$$(NH_4)_2SO_3+S \rightarrow (NH_4)_2S_2O_3 \quad (9)$$

It can also be produced by the reaction of ammonium sulfide, ammonium sulfite, and SO_2:

$$2\ (NH_4)_2S+(NH_4)_2SO_3+3\ SO_2 \rightarrow 3\ (NH_4)_2S_2O_3 \quad (10)$$

Table 7 shows the H_2S conversion and product selectivity (S-SO_2, S-S, S-ATS) at different temperatures for the 3 wt% Nb/Fe-PILC catalyst. These data were obtained after 6 h of reaction. The H_2S conversion was close to 100% in the 220-300 °C temperature range. Much less SO_2 emission was observed over this temperature range. In our previous study [35], we reported that some amount of SO_2 was formed during the selective catalytic oxidation of H_2S without NH_3. Therefore, in the presence of NH_3, the produced SO_2 can react to form $(NH_4)_2SO_3$ according to Eq. (7) and produce ATS as per Eq. (9), increasing the ATS selectivity.

Fig. 8 shows the XPS spectra of Nb $3d_{3/2}$ and Nb $3d_{5/2}$ for the 3 wt% Nb/Fe-PILC catalyst before and after the reaction. The XPS spectra of the used Nb/Fe-PILC showed that the Nb $3d_{5/2}$ and $3d_{3/2}$ peaks were shifted to lower BE after the reaction. This indicates that fresh catalysts with Nb in the +5 oxidation state are partially reduced after the reaction. The XPS peak of Nb $3d_{5/2}$ for Nb^{4+} is reported to appear at 206 eV [44]. After convolution of the Nb $3d_{5/2}$ peak for the used 3 wt% Nb/Fe-PILC catalyst, approximately 45% of the Nb was changed to +4 oxidation state. This result indicates that a highly oxidized form of niobium (Nb^{5+}) produced some SO_2, and a partially reduced form of Nb was highly selective for the production of elemental sulfur via a redox mechanism.

Table 7. H_2S conversion (X-H_2S) and selectivity to products (S-SO_2, S-S and S-ATS) for 3 wt% Nb/Fe-PILC catalyst at different temperatures with NH_3

Temp. (°C)	X-H_2S (%)	S-SO_2 (%)	S-S (%)	S-ATS (%)
300	99.3	0.1	92	7.9
280	98.8	0.2	92	7.8
260	99.6	0.5	94	5.5
240	99.3	0.6	94	5.4
220	99.0	0.4	96	3.6

Reaction conditions: $H_2S/O_2/NH_3/He$=5/2.5/5/87.5, GHSV=10,000 h^{-1}, cat.=0.5 g, reaction time=2 h

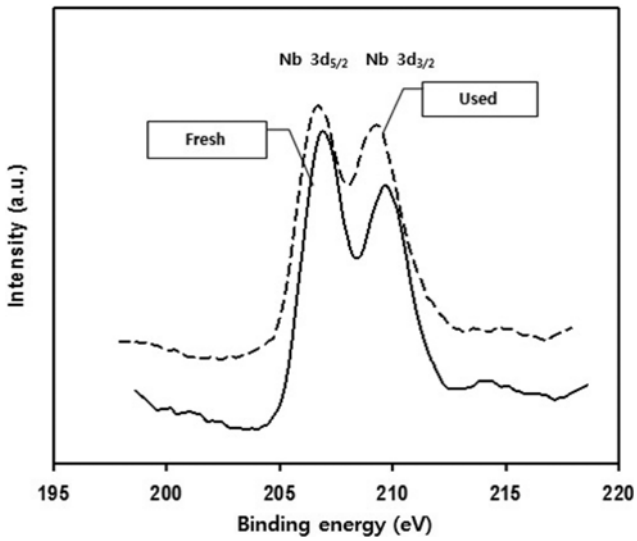

Fig. 8. XPS spectra of Nb $3d_{5/2}$ and Nb $3d_{5/2}$ for the 3 wt% Nb/Fe-PILC catalyst before and after the reaction.

CONCLUSIONS

The catalytic oxidation of H_2S over an Nb/Fe-PILC catalyst with and without NH_3 was investigated. The synthesized catalysts were analyzed using various physico-chemical characterization techniques. The successful pillaring of clay layers by Fe species was confirmed by an increase in the d-spacing, surface area, Fe_2O_3 content, and acidity. Nb/Fe-PILC catalysts exhibited excellent conversion of H_2S with slight SO_2 emission. H_2S was successfully converted to harmless ATS and elemental sulfur. The pillaring of clay layers by Fe_2O_3 increased the surface area of the clay, which facilitated good dispersion of niobium oxides. The conversion of H_2S over Nb/Fe-PILCs with NH_3 increased when the niobium-oxide loading was up to 3 wt%; however, it decreased at higher loadings of niobium oxide because of the formation of crystalline Nb_2O_5. The XPS spectra showed that fresh catalysts with Nb in the +5 oxidation state were partially reduced to a lower oxidation state after the reaction.

ACKNOWLEDGEMENTS

This study was supported by Global Frontier, Global Ph.D. Fellowship and Brain Korea 21 PLUS program of the National Research Foundation of Korea. The authors are also thankful to Pohang Accelerator Laboratory.

REFERENCES

1. J. A. Lagas, J. Borsboom and P. H. Berben, *Oil Gas J.*, **10**, 68 (1988).
2. Kettner and N. Liermann, *Oil Gas J.*, **11**, 63 (1982).
3. R. Kettner, T. Lubcke and N. Liermann, Eur. Patent, 0078690 (1983).
4. P. F. M. T. van Nisselrooy and J. A. Lagas, *Catal. Today*, **16**, 263 (1993).
5. A. Pieplu, O. Saur and J. C. Lavalley, *Catal. Rev. Sci. Eng.*, **40**, 409 (1998).
6. K. V. Bineesh, D. K. Kim, M. I. Kim and D. W. Park, *Appl. Clay Sci.*, **53**, 204 (2011).
7. D. W. Park, B. K. Park, D. K. Park and H. C. Woo, *Appl. Catal. A*, **223**, 215 (2002).
8. D. W. Park, B. K. Park, M. I. Kim, I. Kim and H. C. Woo, *Catal. Today*, **93-95**, 235 (2004).
9. M. I. Kim, D. W. Park, S. W. Park, X. Yang, J. S. Choi and D. J. Suh, *Catal. Today*, **111**, 212 (2006).
10. D. R. Choi, S. Y. Kim, D. W. Park and P. H. Mutin, *Korean J. Chem. Eng.*, **26**, 377 (2009).
11. A. Gil, L. M. Gandia and M. A. Vicente, *Catal. Rev. Sci. Eng.*, **42**, 145 (2000).
12. J. T. Kloprogge, *J. Porous Mater.*, **5**, 5 (1998).
13. K. V. Bineesh, D. K. Kim, M. I. Kim, M. Selvaraj and D. W. Park, *Dalton Trans.*, **40**, 3938 (2011).
14. J. L. Valverde, A. de. Lucas, P. Sanchez, F. Dorado and A. Romero, *Appl. Catal. B*, **43**, 43 (2003).
15. M. Trombetta, G. Busca, M. Lenarda, L. Storaro, R. Ganzerla, L. Piovesan, A. Jimenez Lopez, M. Alcantara-Rodriguez and E. Rodriguez Castellon, *Appl. Catal. A*, **193**, 55 (2000).
16. T. J. Pinnavaia, M.-S. Tzou, S. D. Landau and R. J. Raythatha, *J. Mol. Catal.*, **27**, 195 (1984).
17. R. Q. Long and R. T. Yang, *J. Catal.*, **196**, 73 (2000).
18. K. Tanabe, *Catal. Today*, **78**, 65 (2003).
19. D. Nguyen-Thanh and T. J. Bandosz, *J. Phys. Chem. B*, **107**, 5812 (2003).
20. K.-T. Li and T.-Y. Chien, *Catal. Lett.*, **57**, 77 (1999).
21. S. Yasyerli, G. Dogu and T. Dogu, *Catal. Today*, **117**, 271 (2006).
22. E. K. Lee, K. D. Jung, O. S. Joo and Y. G. Shul, *Appl. Catal. A*, **284**, 1 (2005).
23. N. Keller, C. Pham-Huu and M. J. Ledoux, *Appl. Catal. A*, **217**, 205 (2001).
24. T. N. Mashapa, J. D. Rademan and M. J. Janse van Vuuren, *Ind. Eng. Chem. Res.*, **46**, 6338 (2007).
25. V. V. Shinkarev, A. M. Glushenkov, D. G. Kuvshinov and G. G. Kuvshinov, *Appl. Catal. B*, **85**, 180 (2009).
26. M. D. Soriano, J. Jimenez Jimenez, P. Concepcion, A. Jimenez Lopez, E. Rodriguez Castellon and J. M. Lopez Nieto, *Appl. Catal. B*, **92**, 271 (2009).
27. D. Long, Q. Chen, W. Qiao, L. Zhan, X. Liang and L. Ling, *Chem. Commun.*, 3898 (2009).
28. K. V. Bineesh, D. K. Kim, D. W. Kim, H. J. Cho and D. W. Park, *Energy Environ. Sci.*, **3**, 302 (2010).
29. K. V. Bineesh, M. I. Kim, M. S. Park, K. Y. Lee and D. W. Park, *Catal. Today*, **175**, 183 (2011).
30. K. V. Bineesh. M. I. Kim, G. H. Lee, M. Selvaraj, K. Hyun and D. W. Park, *J. Ind. Eng. Chem.*, **18**, 1845 (2012).
31. E. G. Rightor, M. S. Tzou and T. J. Pinnavaia, *J. Catal.*, **130**, 29 (1991).
32. F. Dorado, A. de. Lucas, P. B. Garcia, A. Romero and J. L. Valverde, *Appl. Catal. A*, **305**, 189 (2006).
33. J. L. Valverde, A. Romero, R. Romero, P. B. Garcia, M. L. Sanchez and I. Asencio, *Clays Clay Miner.*, **53**, 613 (2005).
34. B. G. Mishra and G. Ganga Rao, *J. Porous Mater.*, **10**, 93 (2003).
35. K. V. Bineesh, S. Y. Kim, B. R. Jermy and D. W. Park, *J. Mol. Catal. A*, **308**, 150 (2009).
36. K. V. Bineesh, D. K. Kim, H. J. Cho and D. W. Park, *J. Ind. Eng. Chem.*, **16**, 593 (2010).
37. M. S. P. Francisco, R. Landers and Y. Gushikem, *J. Solid State Chem.*, **177**, 2432 (2004).
38. V. Boffa, J. E. ten Elshof, R. Garcia and D. H. A. Blank, *Micropor. Mesopor. Mater.*, **118**, 202 (2009).
39. L. T. Arenas, P. C. M. Villis, J. Arguello, R. Landers, E. V. Benvenutti and Y. Gusgukem, *Talanta*, **83**, 241 (2010).
40. K. V. Bineesh, D. R. Cho, S. Y. Kim, B. R. Jermy and D. W. Park, *Catal. Commun.*, **9**, 2040 (2008).
41. N. N. Binitha and S. Sugunan, *Micropor. Mesopor. Mater.*, **93**, 82 (2006).
42. E. M. Hartley and M. J. Matterson, *Ind. Eng. Chem. Fundam.*, **14**, 67 (1975).
43. A. Zey, S. White and D. Johnson, *Chem. Eng. Prog.*, **76**, 76 (1980).
44. F. Moulder, W. F. Stickle, P. E. Sobol and K. D. Bomben, *Handbook of X-ray photoelectron spectroscopy*, Perkin-Elmer Co., USA (1992).